(Preprint) AAS 11-437

SEQUENTIAL PROBABILITY RATIO TEST FOR COLLISION AVOIDANCE MANEUVER DECISIONS BASED ON A BANK OF NORM-INEQUALITY-CONSTRAINED EPOCH-STATE FILTERS

J. R. Carpenter*, F. L. Markley†, K. T. Alfriend‡, C. Wright§, and J. Arcido§

Sequential probability ratio tests explicitly allow decision makers to incorporate false alarm and missed detection risks, and are potentially less sensitive to modeling errors than a procedure that relies solely on a probability of collision threshold. Recent work on constrained Kalman filtering has suggested an approach to formulating such a test for collision avoidance maneuver decisions: a filter bank with two norm-inequality-constrained epoch-state extended Kalman filters. One filter models the null hypothesis that the miss distance is inside the combined hard body radius at the predicted time of closest approach, and one filter models the alternative hypothesis. The epoch-state filter developed for this method explicitly accounts for any process noise present in the system. The method appears to work well using a realistic example based on an upcoming highly-elliptical orbit formation flying mission.

INTRODUCTION

Reference 1 proposed the use of a Sequential Probability Ratio Test (SPRT) to guide the collision avoidance maneuver (CAM) decision process. Such tests explicitly allow decision makers to incorporate false alarm and missed detection risks, and are potentially less sensitive to modeling errors than a procedure that relies solely on a probability of collision threshold. Some limitations of the method proposed in Reference 1 include assumptions that the observations are statistically independent, and its reliance on a set of assumptions that reduce the complexity of the encounter.

Recent work on constrained Kalman filtering has suggested an alternative approach to formulating an SPRT for CAM decisions. In our new approach, we introduce a slack variable into Zanetti et al.'s[2] norm-constrained Extended Kalman Filter (EKF) so that it can handle inequality constraints. Then, we set up a filter bank with two norm-inequality-constrained epoch-state EKF's: one for the null hypothesis that the miss distance is inside the combined hard body radius (HBR) at the predicted time of closest approach, and one for the alternative hypothesis. The densities governing the innovations of these two filters form a likelihood ratio for an SPRT.

PROBLEM DESCRIPTION

Given a set of measurements $\mathbb{Y}_{1:k} = \{y_1, y_2, \ldots, y_k\}$ that relate the trajectories of two space objects, we seek to define a procedure that will guide a decision on whether or not to maneuver

*Aerospace Engineer, Navigation and Mission Design Branch, NASA GSFC, Greenbelt, MD 20771.
†Emeritus Aerospace Engineer, Attitude Control Systems Engineering Branch, NASA GSFC, Greenbelt, MD 20771.
‡TEES Distinguished Research Chair Professor, Texas A&M University, College Station, TX 77843.
§a. .i. solutions, Inc.,10001 Derekwood Lane, Suite 215, Lanham, MD 20706.

them to avoid an undesirably close encounter at the time of closest approach t_*. We assume these measurements are given at times $t_k < t_*$ by known m_k-dimensional functions h_k of some n-dimensional state vector $x(t_k)$, corrupted by zero-mean white Gaussian measurement noise v_k:

$$y_k = h_k(x(t_k), t_k) + v_k \tag{1}$$

where orbital parameters of the space objects and any dynamics and/or measurement biases that we wish to estimate are contained within the state vector, and where $\mathrm{E}\left[v_k v_j^T\right] = R_k \delta_{kj}$. We consider the separation between the two objects to be undesirably close whenever the norm of the relative position vector at the time of closest approach, r_*, is less than the combined hard body radius of the two objects, whose value we denote by $\mathcal{R}$. A key assumption is that the true value of $\|r_*\|$ cannot vary sufficiently during the period of observation that it could possibly migrate from inside $\mathcal{R}$ to outside $\mathcal{R}$. Finally, we wish the decision procedure to meet specified rates of false alarms and missed detections.

PROBLEM SOLUTION

There are three threads in our problem solution: a sequential probability ratio test based on the filter innovations, norm-inequality-constrained filtering, and epoch-state filtering. A synthesis of these results yields our solution to the decision problem.

Sequential Probability Ratio Test Based on Filter Innovations

As in Reference 1, our proposed solution is based on Wald's SPRT.[3] In the work we present here, the SPRT uses a ratio of the joint probability densities of the set of measurements $\mathbb{Y}_{1:k}$ under the alternative hypothesis, $\mathcal{H}_1$ that the conjunction is safe, and the null hypothesis, $\mathcal{H}_0$, that the conjunction is unsafe:

$$\Lambda_k = \frac{p\left(\mathbb{Y}_{1:k}|\mathcal{H}_1\right)}{p\left(\mathbb{Y}_{1:k}|\mathcal{H}_0\right)} = \frac{p\left(\mathbb{Y}_{1:k}|r_*^T r_* > \mathcal{R}\right)}{p\left(\mathbb{Y}_{1:k}|r_*^T r_* \leq \mathcal{R}\right)} \tag{2}$$

In a Wald test, one compares Λ_k to decision limits A and B such that whenever $B < \Lambda_k < A$ one should, if possible, seek another observation. If $\Lambda_k \leq B$, then one should accept the null hypothesis, and in the present case, we would recommend a collision avoidance maneuver. If $\Lambda_k \geq A$, then one should accept the alternative hypothesis, and hence we would dismiss the conjunction alarm. Wald's explanations for the thresholds A and B are that we will accept the alternative hypothesis if it is A times more likely than the null, and accept the null hypothesis if it is $1/B$ times more likely than the alternative. Wald shows that such a procedure will terminate with probability one, and that

$$A \leq \frac{1 - P_{fa}}{P_{md}} \text{ and } B \geq \frac{P_{fa}}{1 - P_{md}} \tag{3}$$

where P_{fa} is the allowable false alarm probability, and P_{md} is the allowable missed detection probability.

We assume that the joint density of the measurements can be written in terms of estimates from some sequential estimation procedure, such as the usual Kalman filter:

$$p\left(\mathbb{Y}_{1:k}\right) = p\left(y_k|\hat{x}_{k|k-1}\right) p\left(y_{k-1}|\hat{x}_{k-1|k-2}\right) \cdots p\left(y_1|\hat{x}_{1|0}\right) p\left(\hat{x}_0\right) \tag{4}$$

where $p\left(y_k|\hat{x}_{k|k-1}\right)$ is the density of the k-th measurement conditioned on the estimate incorporating measurements $\mathbb{Y}_{1:k-1}$, and $p\left(\hat{x}_0\right)$ is given. As standard texts, such as Brown and Hwang,[4] show, if the inputs to the estimator are zero-mean and Gaussian, then

$$p\left(y_k|\hat{x}_{k|k-1}\right) = N\left(y_k - h(\hat{x}_{k|k-1}), H_k P_{k|k-1} H_k^T + R_k\right) \tag{5}$$

where $y_k - h(\hat{x}_{k|k-1}) \equiv \varepsilon_{k|k-1}$ is the kth filter innovation, $H_k P_{k|k-1,\mathcal{H}_i} H_k^T + R_k \equiv W_{k|k-1}$ is the innovations covariance, $P_{k|k-1}$ is the filter's error covariance corresponding to $\hat{x}_{k|k-1}$, and $H_k = \partial h_k / \partial x_k|_{\hat{x}_{k|k-1}}$.

If we now suppose the existence of a pair of norm-inequality constrained epoch-state filters, one of which estimates the state at t_* under the constraint that $\mathcal{H}_1 : r_*^T r_* > \mathcal{R}$, and the other under the complementary constraint $\mathcal{H}_0 : r_*^T r_* \leq \mathcal{R}$, then we can write the likelihood ratio in terms of these estimates as follows:

$$\begin{aligned}
\Lambda_k &= \frac{p\left(y_k|\hat{x}_{k|k-1,\mathcal{H}_1}\right) p\left(y_{k-1}|\hat{x}_{k-1|k-2,\mathcal{H}_1}\right) \cdots p\left(y_1|\hat{x}_{1|0,\mathcal{H}_1}\right) p\left(\hat{x}_{0,\mathcal{H}_1}\right)}{p\left(y_k|\hat{x}_{k|k-1,\mathcal{H}_0}\right) p\left(y_{k-1}|\hat{x}_{k-1|k-2,\mathcal{H}_0}\right) \cdots p\left(y_1|\hat{x}_{1|0,\mathcal{H}_0}\right) p\left(\hat{x}_{0,\mathcal{H}_0}\right)} \\
&= \frac{N\left(y_k - h(\hat{x}_{k|k-1,\mathcal{H}_1}), H_k P_{k|k-1,\mathcal{H}_1} H_k^T + R_k\right)}{N\left(y_k - h(\hat{x}_{k|k-1,\mathcal{H}_0}), H_k P_{k|k-1,\mathcal{H}_0} H_k^T + R_k\right)} \Lambda_{k-1} \\
&= \frac{N\left(\varepsilon_{k|k-1,\mathcal{H}_1}, W_{k|k-1,\mathcal{H}_1}\right)}{N\left(\varepsilon_{k|k-1,\mathcal{H}_0}, W_{k|k-1,\mathcal{H}_0}\right)} \Lambda_{k-1},
\end{aligned} \tag{6}$$

where $(\cdot)_{k|k-1,\mathcal{H}}$ denotes the quantity $(\cdot)_k$ conditioned on the *a priori*, on the prior observations, and on the hypothesis $\mathcal{H}$. In the next two subsections, we derive filters suitable for such a test.

Norm-Inequality-Constrained Filtering

Reference 2 derives the norm-equality-constrained Kalman filter by appending a norm constraint on the state vector to the usual Kalman filter cost function. We can convert the norm equality constraint to an inequality constraint through the use of a slack variable α, as described for example by Hull.[5] To this end, let the cost function to minimize be

$$\begin{aligned}
J_k = &\operatorname{tr}\left[P_{k|k-1} - K_{k|k} H_k P_{k|k-1} - P_{k|k-1} H_k^T K_{k|k}^T + K_{k|k} W_{k|k-1} K_{k|k}^T\right] \\
&+ \lambda_k \left[\varepsilon_{k|k-1}^T K_{k|k}^T K_{k|k} \varepsilon_{k|k-1} + 2\varepsilon_{k|k-1}^T K_{k|k}^T \hat{x}_{k|k-1}^T + \hat{x}_{k|k-1} \hat{x}_{k|k-1}^T - \ell + \alpha^2\right]
\end{aligned} \tag{7}$$

where $\operatorname{tr}[\cdot]$ is the trace, $K_{k|k}$ is the usual Kalman gain matrix, and $\ell = \hat{x}^T \hat{x}$ is the norm constraint.*

The constraint equation along with the partial derivatives of the augmented cost function with respect to the Kalman gain and slack variable lead to a set of three equations and three unknowns. As Reference 5 shows, optimality conditions on the constraint boundary correspond to the solution $\alpha = 0$, and optimality conditions off the boundary correspond to $\lambda_k = 0$. Optimality conditions off the boundary ($\lambda_k = 0$) are given by the usual unconstrained Kalman filter solution, which we denote by $\hat{x}_{k|k}$ and $P_{k|k}$. The solution on the constraint boundary ($\alpha = 0$) is given by Reference 2:

$$\hat{x}_{k|k,\|\hat{x}_{k|k}\|=\sqrt{\ell}} = \frac{\sqrt{\ell}}{\left\|\hat{x}_{k|k}\right\|} \hat{x}_{k|k} \tag{8}$$

*The unusual notation for the Kalman gain matrix is for consistency with Appendix A.

$$P_{k|k,\|\hat{x}_{k|k}\|=\sqrt{\ell}} = P_{k|k} + \frac{1}{\varepsilon_{k|k-1}^T W_{k|k-1}^{-1} \varepsilon_{k|k-1}} \left(1 - \frac{\sqrt{\ell}}{\|\hat{x}_{k|k}\|}\right)^2 \hat{x}_{k|k} \hat{x}_{k|k}^T \tag{9}$$

Reference 2 also shows that if the constraint applies to only a subset of the state elements, then the optimal solution for the remaining elements is just the unconstrained Kalman filter solution for those elements.

Epoch-State Filtering

For the problem at hand, the constraint applies only at the time of closest approach, t_*, where $t_* > t_k$, so one may use an epoch-state filter that sequentially processes the set of currently available measurements:

$$\hat{x}_{*|k} = \hat{x}_{*|k-1} + K_{k|k} \varepsilon_{k|k-1} \tag{10}$$

In Appendix A, we show that the optimal gain for this filter is

$$\begin{aligned} K_{k|k} &= \left(P_{*|k-1} - Q_{*,k}\right) \tilde{H}_k^T \left[\tilde{H}_k \left(P_{*|k-1} - Q_{*,k}\right) \tilde{H}_k^T + R_k\right]^{-1} \\ &= \left(P_{*|k-1} - Q_{*,k}\right) \tilde{H}_k^T W_{*|k-1}^{-1} \end{aligned} \tag{11}$$

and the error covariance at epoch is given by

$$P_{*|k} = P_{*|k-1} - K_{k|k} \tilde{H}_k \left(P_{*|k-1} - Q_{*,k}\right) \tag{12}$$

where $\tilde{H}_k = H_k \Phi(t_k, t_*)$ and $Q_{*,k}$ is the process noise density integrated *forward* from t_k to the epoch time t_*, i.e.,

$$Q_{*,k} = \int_{t_k}^{t_*} \Phi(t_*, \tau) Q(\tau) \Phi^T(t_*, \tau) \mathrm{d}\tau \tag{13}$$

Synthesis

We are now in a position to synthesize the results above. Application of the constraint to the *a priori* state and covariance yields:

$$\hat{r}_{*|0,\mathcal{H}_1} = \begin{cases} \hat{r}_{*|0} & \text{if } \|\hat{r}_{*|0}\| > \mathcal{R} \\ \frac{\mathcal{R}}{\|\hat{r}_{*|0}\|} \hat{r}_{*|0} & \text{otherwise} \end{cases} \tag{14}$$

$$\hat{r}_{*|0,\mathcal{H}_0} = \begin{cases} \hat{r}_{*|0} & \text{if } \|\hat{r}_{*|0}\| \leq \mathcal{R} \\ \frac{\mathcal{R}}{\|\hat{r}_{*|0}\|} \hat{r}_{*|0} & \text{otherwise} \end{cases} \tag{15}$$

$$P_{rr_{*|0,\mathcal{H}_1}} = \begin{cases} P_{rr_{*|0}} & \text{if } \|\hat{r}_{*|0}\| > \mathcal{R} \\ P_{rr_{*|0}} + \left(1 - \frac{\mathcal{R}}{\|\hat{r}_{*|0}\|}\right)^2 \hat{r}_{*|0} \hat{r}_{*|0}^T & \text{otherwise} \end{cases} \tag{16}$$

$$P_{rr_{*|0,\mathcal{H}_0}} = \begin{cases} P_{rr_{*|0}} & \text{if } \|\hat{r}_{*|0}\| \leq \mathcal{R} \\ P_{rr_{*|0}} + \left(1 - \frac{\mathcal{R}}{\|\hat{r}_{*|0}\|}\right)^2 \hat{r}_{*|0} \hat{r}_{*|0}^T & \text{otherwise} \end{cases} \tag{17}$$

The remaining elements of the state and covariance are unaffected by the constraint application.

The kth measurement update, under each hypothesis, $\mathcal{H}_i$, is as follows:

$$\hat{x}_{*|k,\mathcal{H}_i} = \hat{x}_{*|k-1,\mathcal{H}_i} + K_{k|\mathcal{H}_i}\varepsilon_{k|k-1,\mathcal{H}_i} \tag{18}$$

$$P_{*|k,\mathcal{H}_i} = P_{*|k-1,\mathcal{H}_i} - K_{k|\mathcal{H}_i}\tilde{H}_k\left(P_{*|k-1,\mathcal{H}_i} - Q_{*,k}\right) \tag{19}$$

$$\begin{aligned} K_{k|\mathcal{H}_i} &= \left(P_{*|k-1,\mathcal{H}_i} - Q_{*,k}\right)\tilde{H}_k^T\left[\tilde{H}_k\left(P_{*|k-1,\mathcal{H}_i} - Q_{*,k}\right)\tilde{H}_k^T + R_k\right]^{-1} \\ &= \left(P_{*|k-1,\mathcal{H}_i} - Q_{*,k}\right)\tilde{H}_k^T W_{k|k-1,\mathcal{H}_i}^{-1} \end{aligned} \tag{20}$$

Application of the constraint to the *a posteriori* state and covariance yields:

$$\hat{r}_{*|k,\mathcal{H}_1} \leftarrow \begin{cases} \hat{r}_{*|k,\mathcal{H}_1} & \text{if } \left\|\hat{r}_{*|k,\mathcal{H}_1}\right\| > \mathcal{R} \\ \dfrac{\mathcal{R}}{\left\|\hat{r}_{*|k,\mathcal{H}_1}\right\|}\hat{r}_{*|k,\mathcal{H}_1} & \text{otherwise} \end{cases} \tag{21}$$

$$\hat{r}_{*|k,\mathcal{H}_0} \leftarrow \begin{cases} \hat{r}_{*|k,\mathcal{H}_0} & \text{if } \left\|\hat{r}_{*|k,\mathcal{H}_0}\right\| \leq \mathcal{R} \\ \dfrac{\mathcal{R}}{\left\|\hat{r}_{*|k,\mathcal{H}_0}\right\|}\hat{r}_{*|k,\mathcal{H}_0} & \text{otherwise} \end{cases} \tag{22}$$

$$P_{rr_{*|k,\mathcal{H}_1}} \leftarrow \begin{cases} P_{rr_{*|k,\mathcal{H}_1}} & \text{if } \left\|\hat{r}_{*|k,\mathcal{H}_1}\right\| > \mathcal{R} \\ P_{rr_{*|k,\mathcal{H}_1}} + \dfrac{1}{\tilde{\varepsilon}_{k|k-1,\mathcal{H}_1}}\left(1 - \dfrac{\mathcal{R}}{\left\|\hat{r}_{*|k,\mathcal{H}_1}\right\|}\right)^2 \hat{r}_{*|k,\mathcal{H}_1}\hat{r}_{*|k,\mathcal{H}_1}^T & \text{otherwise} \end{cases} \tag{23}$$

$$P_{rr_{*|k,\mathcal{H}_0}} \leftarrow \begin{cases} P_{rr_{*|k,\mathcal{H}_0}} & \text{if } \left\|\hat{r}_{*|k,\mathcal{H}_0}\right\| > \mathcal{R} \\ P_{rr_{*|k,\mathcal{H}_0}} + \dfrac{1}{\tilde{\varepsilon}_{k|k-1,\mathcal{H}_0}}\left(1 - \dfrac{\mathcal{R}}{\left\|\hat{r}_{*|k,\mathcal{H}_0}\right\|}\right)^2 \hat{r}_{*|k,\mathcal{H}_0}\hat{r}_{*|k,\mathcal{H}_0}^T & \text{otherwise} \end{cases} \tag{24}$$

where

$$\tilde{\varepsilon}_{k|k-1,\mathcal{H}_i} = \varepsilon_{k|k-1,\mathcal{H}_i}^T W_{k|k-1,\mathcal{H}_1}^{-1}\varepsilon_{k|k-1,\mathcal{H}_i} \tag{25}$$

The remaining elements of the state and covariance are unaffected by the constraint application.

Finally, the likelihood ratio updates as follows:

$$\Lambda_k = \frac{N\left(\varepsilon_{k|k-1,\mathcal{H}_1}, W_{k|k-1,\mathcal{H}_1}\right)}{N\left(\varepsilon_{k|k-1,\mathcal{H}_0}, W_{k|k-1,\mathcal{H}_0}\right)}\Lambda_{k-1} \tag{26}$$

EXAMPLES

We use two examples to illustrate our method. The first example is a gross simplification of the close approach scenario, but it gives good insight into how the method works. The second example is more realistic, using a close approach found during one of the high-fidelity end-to-end mission simulations recently conducted by the flight dynamics team for the Magnetospheric Multi-Scale formation flying mission (MMS).

Simple Example

Our simple example is a static two-dimensional problem. The true miss distance is chosen from one of four cases: (1) a "clear hit," when the true miss distance is well inside $\mathcal{R}$; (2) a "near hit," when the true miss distance is close to, but inside, $\mathcal{R}$; (3) a "near miss," when the true miss distance is close to, but outside, $\mathcal{R}$; and (4) a "clear miss," when the true miss distance is well outside the $\mathcal{R}$ (but still close enough for concern). The epoch-state filter bank processes measurements of the relative position components, which are corrupted by zero-mean Gaussian white noise with standard deviation $\mathcal{R}/4$. The filters assume initial standard deviations of $3\mathcal{R}$. No process noise is modeled.

Figures 1 – 4 depict results for each case. The upper left subplot of each figure shows the conjunction geometry and the filter bank's estimates. The combined hard body radius is a dashed blue circle, and the true radius of closest approach is marked with a black '+' symbol. The sequence of estimated relative positions and corresponding error covariances for each filter in the bank are shown in this subplot, respectively, by the symbol 'o' and a surrounding 1σ error ellipse, and colored red for the null hypothesis filter, and green for the alternative hypothesis filter. The upper right and lower left subplots of each figure show the filters innovations and their 1σ formal errors as solid and dashed lines, respectively, colored red for the null and green for the alternative hypothesis filters. Finally, each figure shows the likelihood ratio and corresponding decision boundaries in the lower right subplot, the latter of which are the equalities from Eq. 3. In this subplot, the likelihood ratio is a blue line, and the upper green boundary corresponds to guidance to dismiss the conjunction, while the red lower boundary corresponds to guidance to maneuver. These decision boundaries are based on an allowable false alarm probability of one in twenty, and missed detection probability of one in one thousand.

The effect of applying the constraint to the filters is clearly evident in the upper left subplots: the filter which has the correct hypothesis quickly converges to the true value and its covariance ellipse rapidly shrinks to a small circle, while the filter with the incorrect hypothesis hovers around the boundary, and its covariance ellipse gets elongated along the radial direction in which the constraint was applied.

Figure 1–4 illustrate just one case of each type, but we have run 10,000-case Monte Carlo trials for each of the four categories of conjunction, finding no false alarms and no missed detections.

MMS Example

Figure 5 depicts the scenario of the MMS example. During this mission phase, known as "Phase 2b," MMS will be in a 1.2 by 25 earth radii (R_E) elliptical orbit, with a nominal separation at apogee between the four spacecraft that varies between 25 and 40 km. The large loops evident in the upper subplot of Figure 5, during which the formation is roughly co-planar, occur around perigee, and the plane crossings occur roughly at altitudes of two to three R_E, near where the spacecraft cross the semi-latus recta of their orbits. Collisions are most likely to occur near perigee, shown as the sharp minima in the lower subplot of Figure 5 .

To create our test case, we extracted Brower-Lyddane mean orbital elements from the MMS end-to-end simulation at the time of closest approach. To create our simulation truth, we then back-propagated the formation for two orbital revolutions using the Gim-Alfriend state transition matrix,[6] which accounts for both high eccentricity and Earth oblateness. The latter is the primary perturbation of the MMS relative motion.

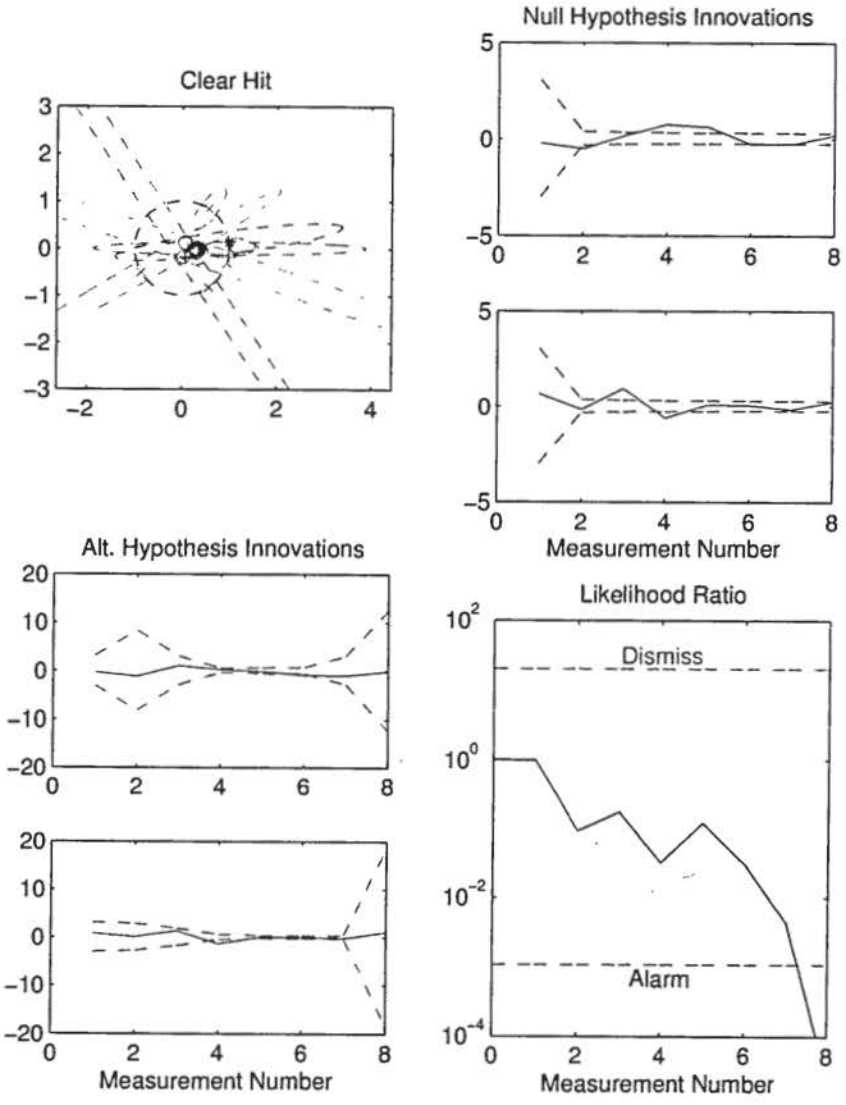

Figure 1. Simple example clear hit test case with actual miss distance $3\mathcal{R}/16$. Distance units are normalized to $\mathcal{R}$.

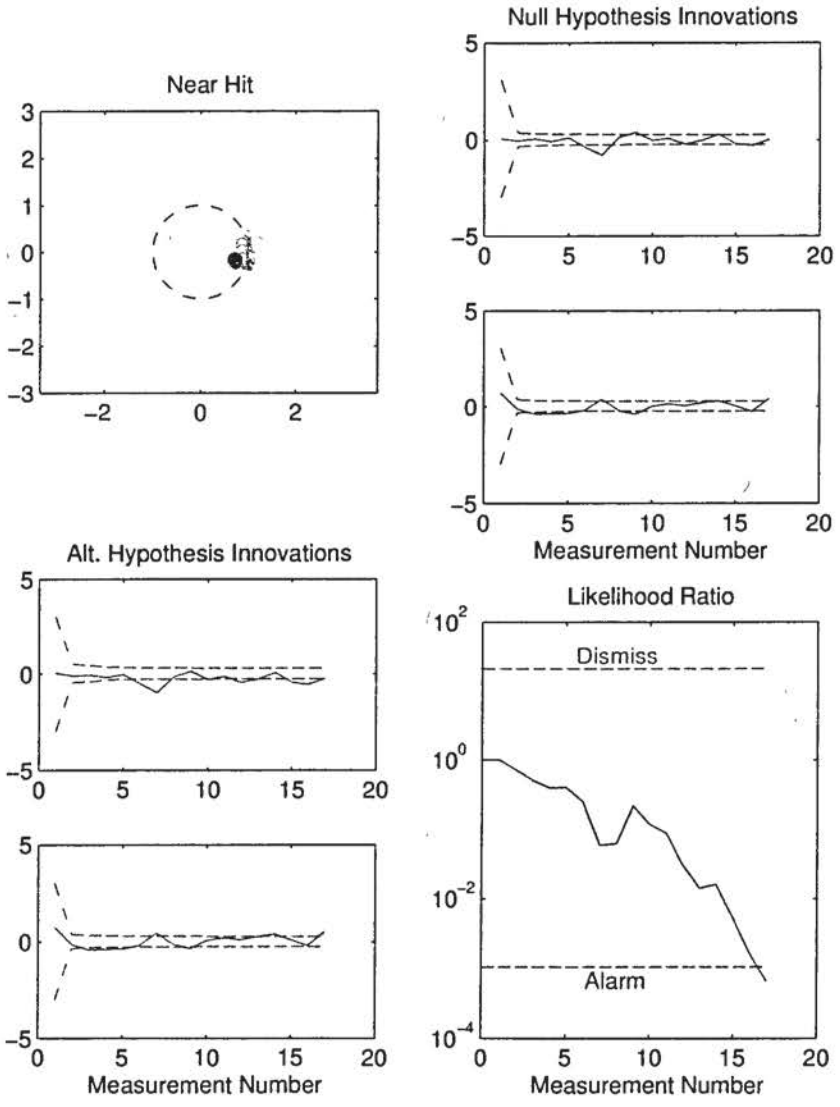

Figure 2. Simple example near hit test case with actual miss distance $3\mathcal{R}/4$. Distance units are normalized to $\mathcal{R}$.

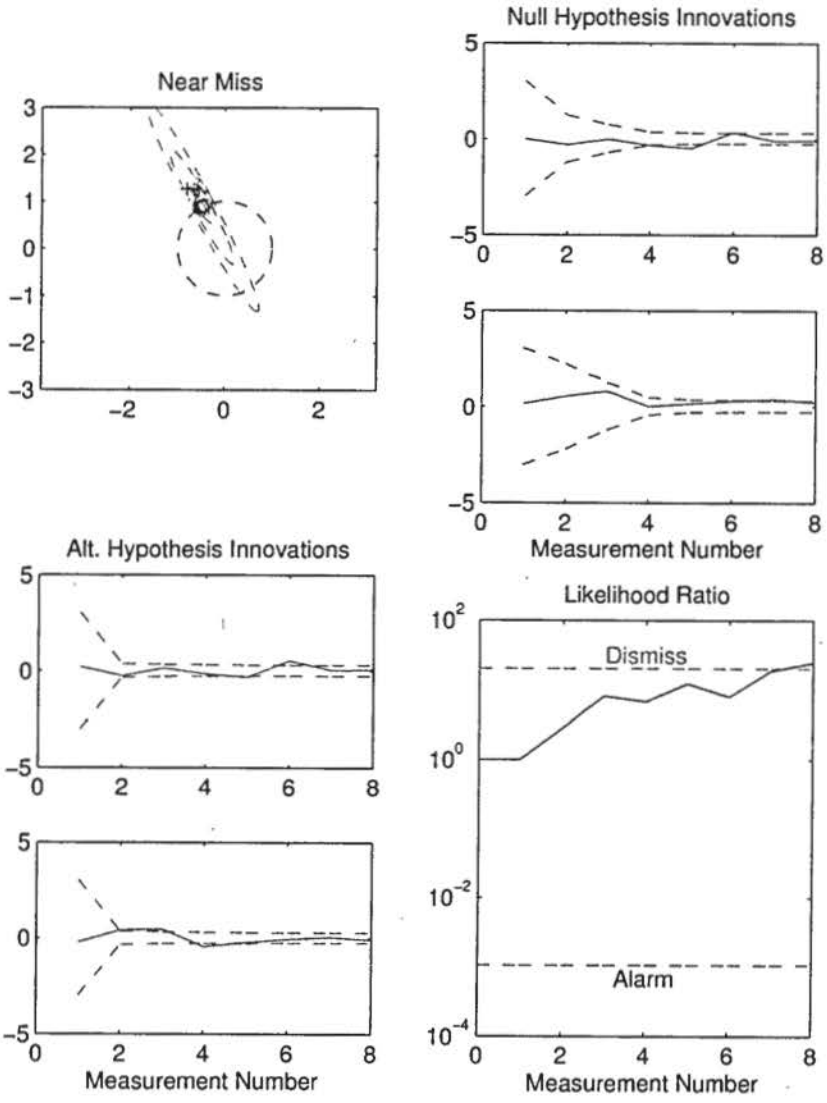

Figure 3. Simple example near miss test case with actual miss distance $3\mathcal{R}/2$. Distance units are normalized to $\mathcal{R}$.

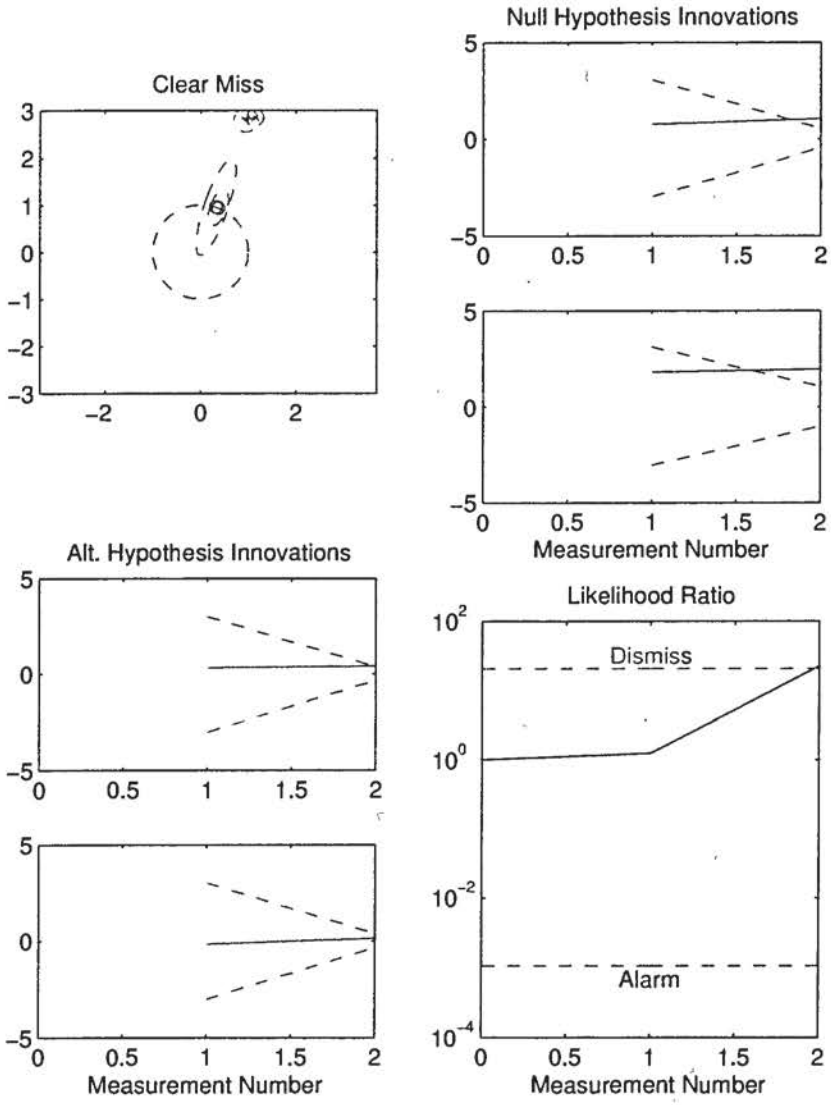

Figure 4. Simple example clear miss test case with actual miss distance $3\mathcal{R}$. Distance units are normalized to $\mathcal{R}$.

We next simulated a simplified version of the MMS navigation process. Here, we simulated measurements of the relative position vector between the two satellites involved in the conjunction. These measurements were corrupted by white noise with standard deviation of 10 m, and by a first-order Gauss-Markov bias process with steady-state standard deviation of 3 m. We simulated these measurements at 60 sec rate.

We processed these observations using an unconstrained filter for just over one orbital period to achieve a converged navigation state. This filter estimated both the relative position/velocity state, and the three components of the Gauss-Markov measurement bias. Then, just after the perigee preceding the close approach, we initiated the Wald test procedure described previously herein, using the converged unconstrained filter solutions. Figures 6 through 9 show our results for four cases that we refer to as the clear hit, near hit, near miss, and clear miss cases.

Figure 6 depicts the clear hit case. The upper left subplot shows a close up of the relative motion over approximately an hour preceding the closest approach. For this case, we set $\mathcal{R} = 1.5$ km, which significantly exceeds the actual separation of 0.5 km at t_*. We mark the epoch-state position solutions from the null hypothesis (red) and alternative hypothesis (green) filters on this plot. One can see the green solutions reside on the constraint boundary (shown as a grey sphere), while the red solutions cluster near the true relative position, inside the boundary. The upper-right and lower-left subplots show the estimation errors and their one-sigma formal errors for each of the two constrained filters, with the former showing the filter that assumes the null hypothesis, and the latter showing the filter that assumes the alternative hypothesis. It is clear from these plots that the null hypothesis filter performance is superior. The lower right subplot depicts the log-likelihood ratio, and the decision bounds. Evidently, the superior performance of the null hypothesis filter leads to a rapid and definite decision to maneuver.

Figure 7 depicts the near hit case. For this case, we set $\mathcal{R} = 0.75$ km, which is much closer to, but still exceeds, the actual separation of 0.5 km at the actual separation at t_*. The alternative and null hypothesis solutions are now much closer together, but a rapid and definitive decision to maneuver is still evident.

Figure 8 depicts the near miss case. For this case, we set $\mathcal{R} = 0.33$ km, which is close to, but less than, the actual separation of 0.5 km at the actual separation at t_*. The alternative and null hypothesis solutions are similar, but a bias is evident in the null hypothesis filter, as a consequence of its being forced onto the constraint boundary. This leads to a rapid and definitive decision that a maneuver is not required.

Figure 9 depicts the clear miss case. For this case, we set $\mathcal{R} = 0.12$ km, which is much less than the actual separation of 0.5 km at the actual separation at t_*. The alternative and null hypothesis solutions are similar, but again a bias is evident in the null hypothesis filter, as a consequence of its being forced onto the constraint boundary. This again leads to a rapid and definitive decision that a maneuver is not required.

DISCUSSION

The examples just described suggest that the proposed method provides a useful new tool for conjunction assessment analysis, which is free of some limiting assumption in a similar method we previously proposed in Reference 1. Any final decision to maneuver or dismiss a potential conjunction should obviously take into account all available data on the degree to which the close approach appears to be dangerous. In this section, we describe some additional considerations.

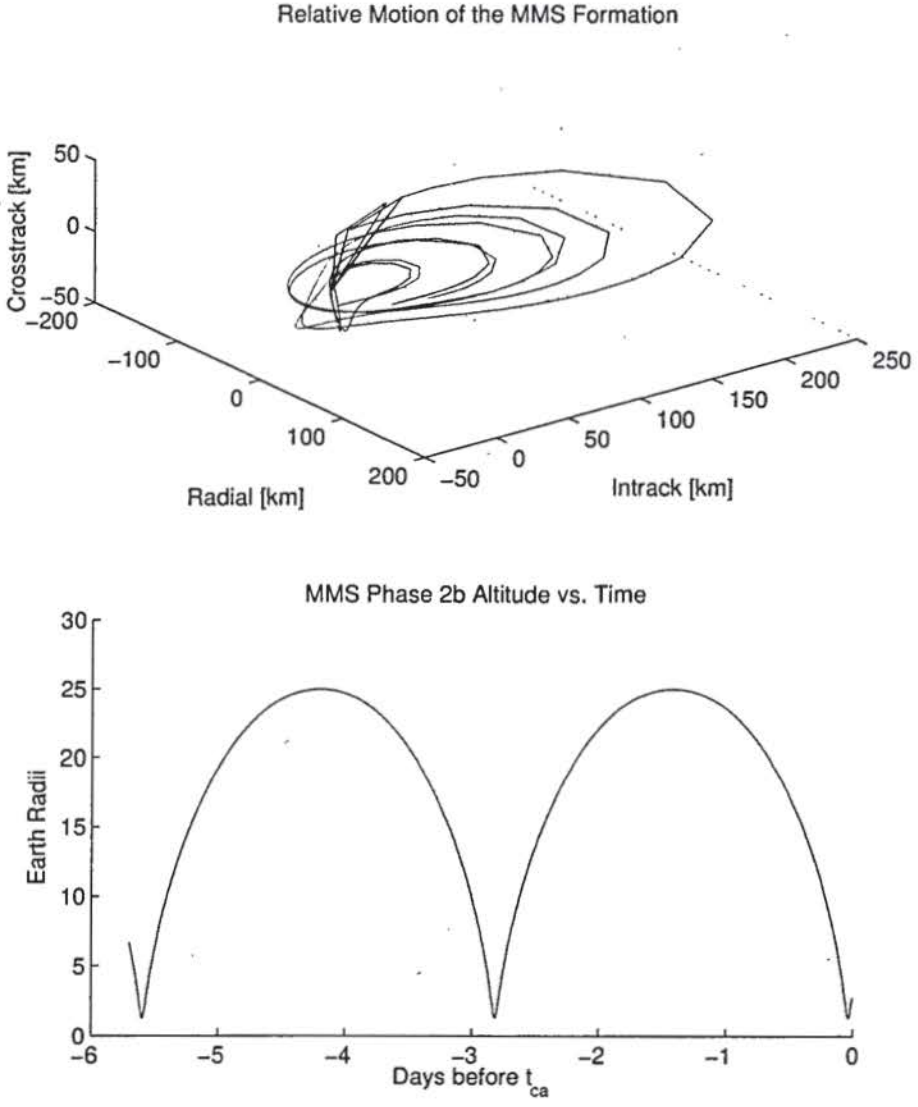

Figure 5. MMS Test Case. In the upper subplot, the black tetrahedron shows the formation at $t_* = 0$; the close approach occurs when the spacecraft illustrated with the blue trace passes within 0.5 km of the spacecraft at the origin. This occurs just prior to the third minimum in the lower subplot. The collision avoidance maneuver decision occurs 2.85 days prior to the event, just after the preceding perigee at the second minimum on the lower subplot.

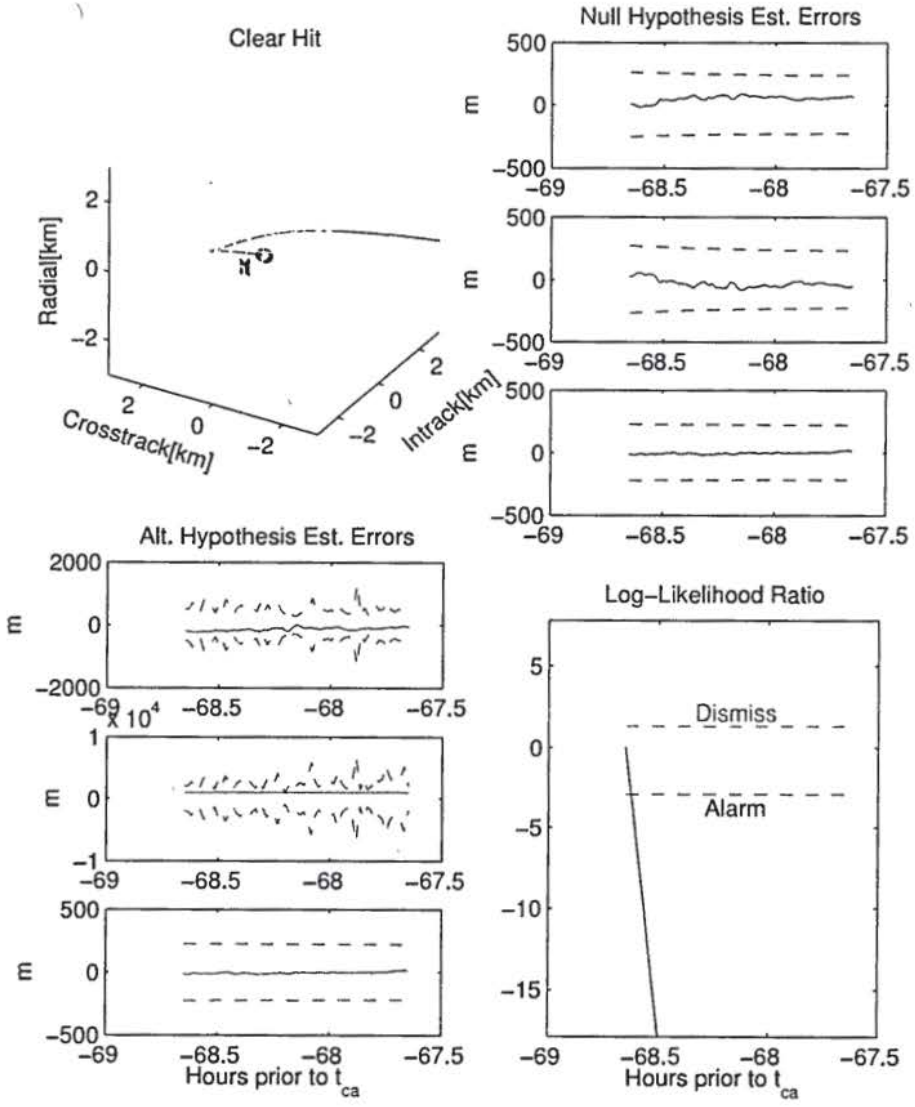

Figure 6. MMS clear hit test case using combined hard body radius of 1.5 km when actual miss distance is 0.5 km.

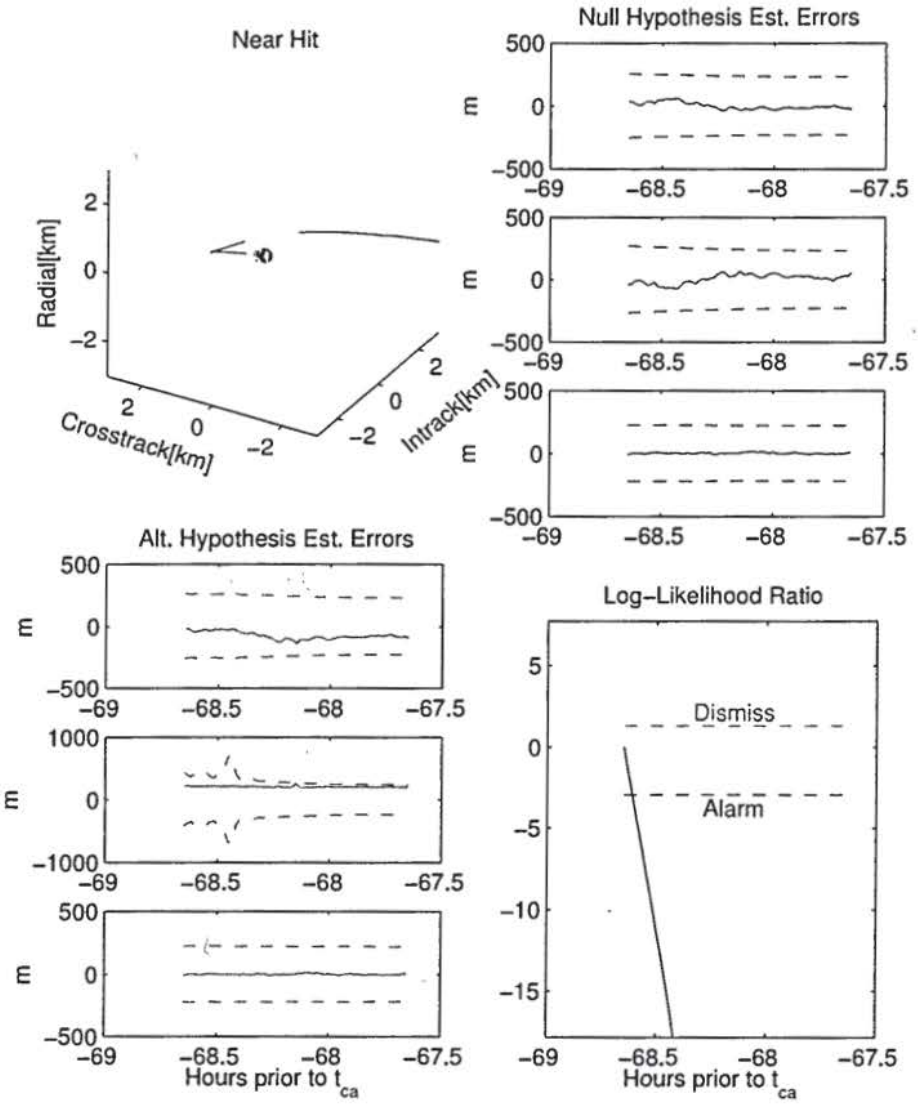

Figure 7. MMS near hit test case using combined hard body radius of 0.75 km when actual miss distance is 0.5 km.

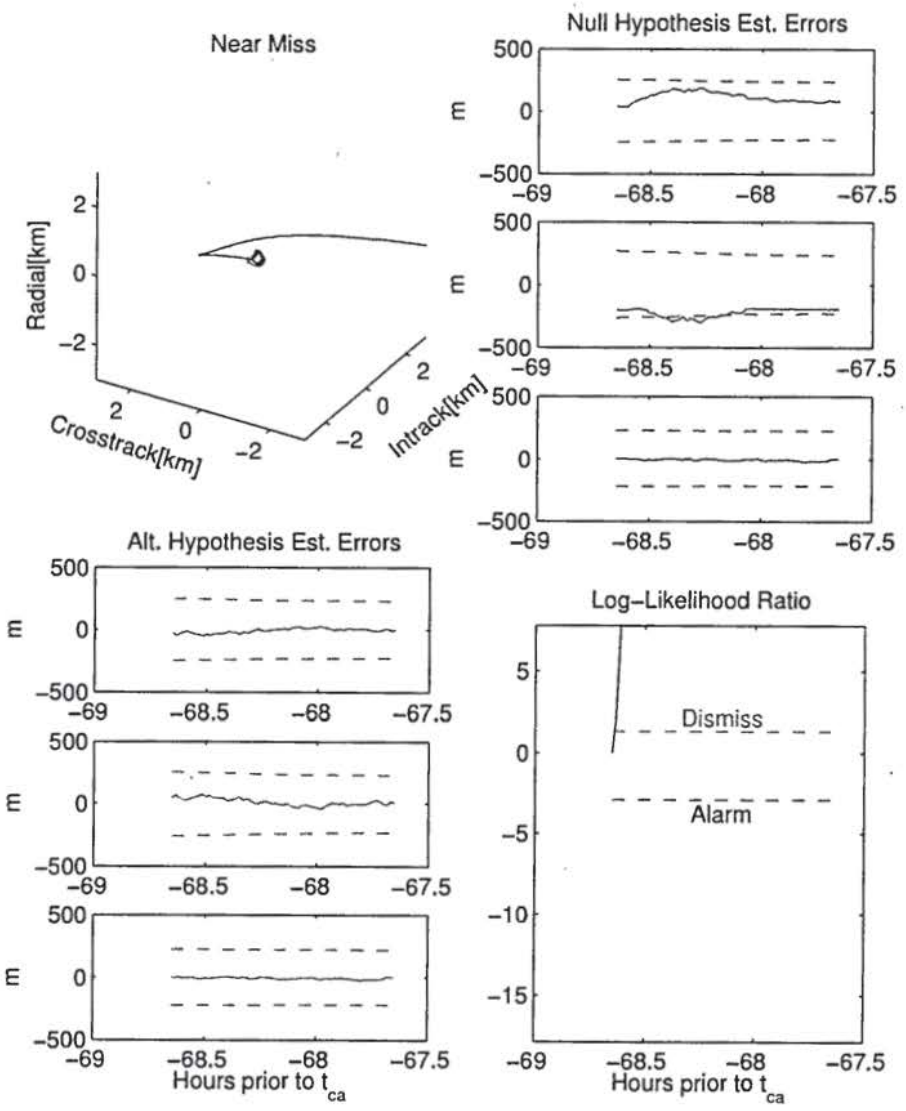

Figure 8. MMS near miss test case using combined hard body radius of 0.33 km when actual miss distance is 0.5 km.

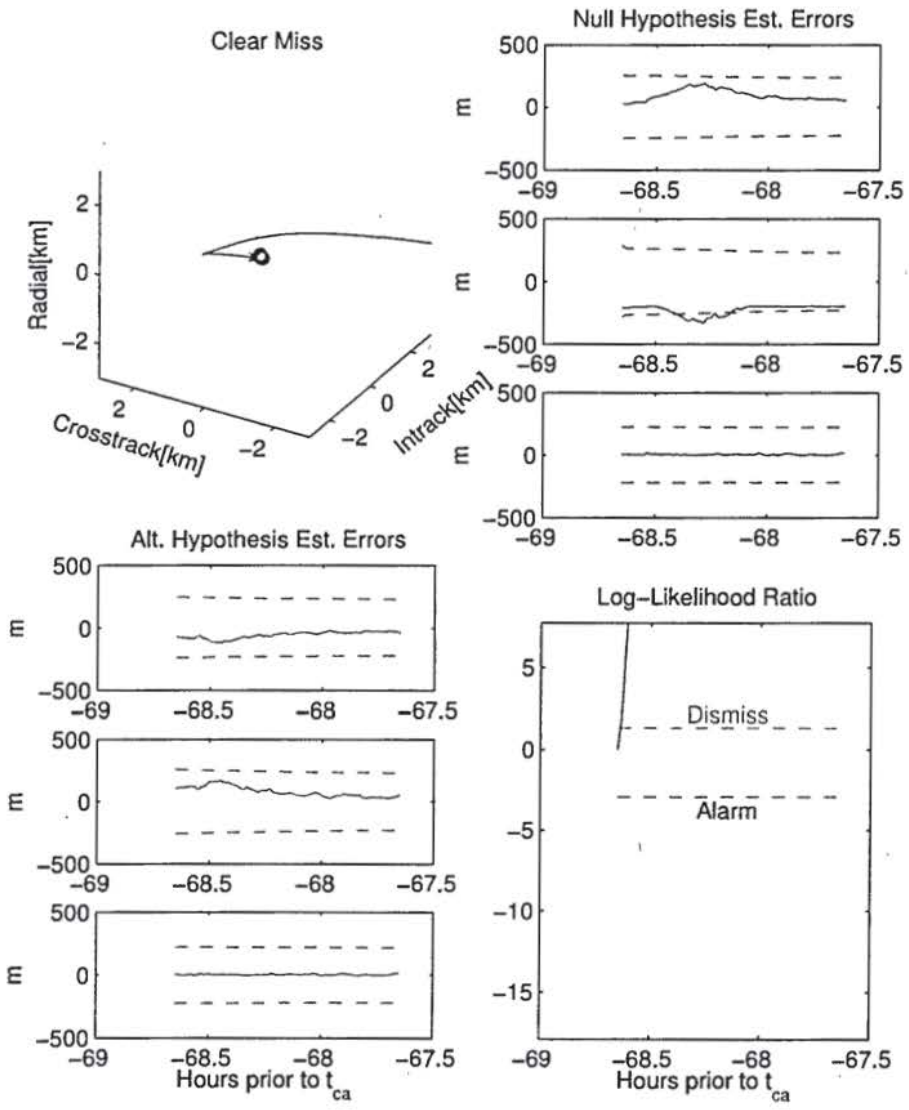

Figure 9. MMS clear miss test case using combined hard body radius of 1.5 km when actual miss distance is 0.12 km.

Our use of a Wald test depends on the assumption that the hypotheses being compared are fixed, which in the present case means that the true value of $\|r_*\|$ is either inside $\mathcal{R}$ or outside $\mathcal{R}$ on a given scenario. If instead we wished to consider that random or unmodeled perturbations could change the true value of $\|r_*\|$ sufficiently to convert a hit into a miss and vice versa during the course of a given scenario, then we would need to use a different test, such as a Shirayeyev test.[7]

In the examples given here, we assumed that the time of closest approach, t_* is known and fixed. It may be more realistic to assume that t_* will change as the estimation process develops greater certainty about the epoch state. This kind of variability in the epoch time has been addressed by Battin et al.,[8] who described an epoch-state filter that implicitly allowed t_* to vary via an additional update of the true anomaly.

Using a pair of estimators for each possible conjunction in a large catalog of space objects could be computationally daunting. Instead, we envision that the filter bank our Wald test requires would be brought online only after some prior screening procedure had already identified a conjunction of concern. One possibility for such a screening process might involve the Mahalanobis metric, such as

$$\sqrt{\hat{r}^T P_{rr}^{-1} \hat{r}} < \chi^{-1}(1 - P_{md}, 3) \tag{27}$$

where $\chi^{-1}(1 - P_{md}, 3)$ is the inverse of the χ distribution with three degrees of freedom corresponding to a complementary probability of P_{md}, the allowable missed detection probability. This procedure would be comparable to a screen based on collision probability, but it does not depend on assumptions about geometry, quadratures, nor other approximations to an integral (except the tabulation of the χ distribution). Unlike a fixed screening volume, a Mahalanobis screen will properly adapt to how the uncertainty changes throughout an orbital prediction. An even simpler screen, which could be used as first step, would be the mean latitude difference screen proposed by Gottlieb et al.[9]

Finally, our present method, like all but the simplest screens, depends on correctly predicting the probability densities at the time of closest approach. If the prediction error distributions are sufficiently close to Gaussians, which can often be achieved through judicious choice of state representation (e.g., using mean elements rather than Cartesian states), then we need merely have sufficiently accurate covariance information and sufficiently unbiased estimates of the mean. A possible advantage of the present method is that it can accommodate any error distribution. Another possible advantage of the present method is that it depends only on the ratio of two densities, and hence might be expected to be more robust than a method that depends on integrating the density over a region that is far out in the density's tail, which is often the case with a collision probability metric.

CONCLUSIONS

In this work, we have developed a new SPRT for collision avoidance. We modified the norm-constrained Extended Kalman Filter (EKF) so that it can handle inequality constraints. Then, we set up a filter bank with two norm-inequality-constrained epoch-state EKF's: one for the null hypothesis that the miss distance is inside the combined hard body radius (HBR) at the predicted time of closest approach, and one for the alternative hypothesis. Our post-measurement epoch-state filter explicitly accommodates process noise, and we use it to estimate the relative states at the time of closest approach. The densities governing the innovations of the two epoch-state filters form a likelihood ratio for our new SPRT. The proposed method appears to provide a useful new tool for conjunction assessment analysis.

APPENDIX A: EPOCH-STATE FILTER WITH PROCESS NOISE

Since their invention by Gauss,[10] batch least-squares estimators have been used to provide epoch state solutions from a set of measurements of orbital bodies. Battin et al.[8] described an epoch-state navigation filter that estimated Cartesian position and velocity at an epoch time t_o that is implicitly allowed to vary via an additional update of the true anomaly. These approaches do not admit the presence of process noise, and hence the epoch time can freely be chosen to be before, during, or after the batch of measurements. Montenbruck[11] developed an epoch-state filter that estimated SGP4 elements,[12] and incorporated a form of process noise, but in a somewhat artificial fashion that was intended primarily to address numerical stability. In Reference 13, two of the present authors described how the effect of process noise on a batch estimator which itself ignored the process noise could be ascertained, for arbitrary placement of the epoch time. However, Reference 13 did not consider the case when the estimator models the effect of process noise in its gain computation*. In this Appendix, we describe a post-measurement batch epoch-state filter that accounts for process noise, which is suitable for any prediction problem where process noise needs to be accommodated. We develop this estimator first in a batch form, then reduce the batch update to recursion suitable for sequential implementation.

Batch Form

A batch filter produces its estimate based on processing a collection of m_i-dimensional measurements y_i, $i = 1, 2, \ldots, N$ made at various times. Combining these measurements into a single vector, we have

$$y = \begin{bmatrix} y_1 \\ \vdots \\ y_N \end{bmatrix}, \quad \hat{y} = \begin{bmatrix} \hat{y}_1 \\ \vdots \\ \hat{y}_N \end{bmatrix}, \quad \varepsilon = y - \hat{y} = \begin{bmatrix} \varepsilon_1 \\ \vdots \\ \varepsilon_N \end{bmatrix} \tag{28}$$

where $\hat{y}$ is the filter's predicted measurement vector, and ε is the filter innovation. The batch filter performs a single update at the epoch time:

$$\hat{x}_{*|N} = \hat{x}_{*|0} + K\varepsilon = \hat{x}_{*|0} + \sum_{i=1}^{N} K_i \varepsilon_i, \tag{29}$$

where $\hat{x}_{*|0}$ is an *a priori* estimate of x_* and K is a gain matrix consisting of a "row" of gain matrices for each measurement, K_i. For the present work, we restrict our attention to the case where $t_* > t_N$.

By assumption, the n-dimensional state vector evolves according to

$$\frac{\mathrm{d}}{\mathrm{d}t} x(t) = f(x(t), t) + w(t) \tag{30}$$

where the process noise $w(t)$ is a Gaussian white noise process with mean and covariance given by

$$\mathrm{E}\left[w(t)\right] = 0_n \quad \text{and} \quad \mathrm{E}\left[w(t)w(\tau)^T\right] = Q(t)\delta(t - \tau), \tag{31}$$

with $\mathrm{E}\left[\cdot\right]$ denoting the expectation operator and 0_n denoting an n-dimensional vector of zeros. In the covariance equation, Q is the $n \times n$ process noise spectral density matrix.

*While preparing this paper, we have discovered errata in Reference 13 that affect the case when the epoch time is not prior to the measurement batch, which we list in Appendix B.

We define the state error vector as $e(t) = x(t) - \hat{x}(t)$, and to first order it evolves according to

$$\frac{\mathrm{d}}{\mathrm{d}t}e(t) = A(t)e(t) + w(t), \tag{32}$$

where

$$A(t) = \left.\frac{\partial f(x(t),t)}{\partial x(t)}\right|_{\hat{x}(t)}. \tag{33}$$

Formal integration of Eq. 32 gives

$$e(t) = \Phi(t,t_i)e_i + w_d(t,t_i) \tag{34}$$

where the state transition matrix, $\Phi(t,t_i)$, is the solution of

$$\dot{\Phi}(t,t_i) = A(t)\Phi(t,t_i) \tag{35}$$

with the initial condition

$$\Phi(t_i,t_i) = I_n = \text{the } n \times n \text{ identity matrix}, \tag{36}$$

and the random excitation vector, $w_d(t,t_i)$, is given by the formal integral

$$w_d(t,t_i) = \int_{t_i}^{t} \Phi(t,\tau)w(\tau)\mathrm{d}\tau. \tag{37}$$

The innovation may be written in terms of the estimation error as

$$\varepsilon_i = H_i e_i + v_i, \tag{38}$$

Substituting Eqs. 34 and 38 into Eq. 28 at the epoch time gives

$$\varepsilon = \tilde{H}e_{*|0} + u_d + v \tag{39}$$

where

$$\tilde{H} = \begin{bmatrix} \tilde{H}_1 \\ \vdots \\ \tilde{H}_N \end{bmatrix} = \begin{bmatrix} H_1\Phi(t_1,t_*) \\ \vdots \\ H_N\Phi(t_N,t_*) \end{bmatrix}, \quad u_d = \begin{bmatrix} u_{d1} \\ \vdots \\ u_{dN} \end{bmatrix} = \begin{bmatrix} H_1 w_d(t_1,t_*) \\ \vdots \\ H_N w_d(t_N,t_*) \end{bmatrix}, \quad v = \begin{bmatrix} v_1 \\ \vdots \\ v_N \end{bmatrix} \tag{40}$$

Using Eqs. 29 and 39, the estimation error after a batch update is

$$e_{*|N} = \left(I_n - \sum_{i=1}^{N} K_i\tilde{H}_i\right)e_{*|0} - \sum_{i=1}^{N} K_i v_i - \sum_{i=1}^{N} K_i u_{di} \tag{41}$$

Since the *a priori* filter state $\hat{x}_{*|0}$ can only have been developed from information available prior to the measurement batch, the *a priori* estimation error propagates from the time of this prior information according to

$$e_{*|0} = \Phi(t_*,t_0)e_{0|0} + w_d(t_*,t_0), \tag{42}$$

where t_0 is some time prior to the epoch time and to all the measurement times. This means that $e_{*|0}$ is correlated with $w_d(t_*,t_0)$, which somewhat complicates the expression for the covariance at

epoch. Omitting the expectations involving zero correlations, we find the epoch-state covariance to be given by

$$P_{*|N} = \mathrm{E}\left[e_{*|N}e_{*|N}^T\right] \tag{43}$$

$$= \left(I_n - \sum_{i=1}^{N} K_i\tilde{H}_i\right)\mathrm{E}\left[e_{*|0}e_{*|0}^T\right]\left(I_n - \sum_{i=1}^{N} K_i\tilde{H}_i\right)^T + \sum_{i=1}^{N} K_i\mathrm{E}\left[v_i v_i^T\right]K_i^T \tag{44}$$

$$+ \sum_{i,j=1}^{N} K_i\mathrm{E}\left[u_{di}u_{dj}^T\right]K_j^T - \sum_{i=1}^{N} K_i\mathrm{E}\left[u_{di}w_d^T(t_*,t_0)\right]\left(I_n - \sum_{j=1}^{N} K_j\tilde{H}_j\right)^T$$

$$- \left(I_n - \sum_{i=1}^{N} K_i\tilde{H}_i\right)\sum_{j=1}^{N}\mathrm{E}\left[w_d(t_*,t_0)u_{dj}^T\right]K_j^T \tag{45}$$

Now, with our assumption that $t_* > t_N$, we find that

$$\begin{aligned}\mathrm{E}\left[u_{di}u_{dj}^T\right] &= H_i\mathrm{E}\left[w_d(t_i,t_*)w_d^T(t_j,t_*)\right]H_j^T \\ &= H_i\int_{t_*}^{t_j}\int_{t_*}^{t_i}\Phi(t_i,\tau)Q(\tau)\delta(\tau-\tau')\Phi^T(t_j,\tau')\mathrm{d}\tau\mathrm{d}\tau' H_j^T \\ &= \tilde{H}_i\,Q_{*,\max(i,j)}\,\tilde{H}_j^T\end{aligned} \tag{46}$$

Similarly

$$\begin{aligned}\mathrm{E}\left[u_{di}w_d^T(t_*,t_0)\right] &= H_i\mathrm{E}\left[w_d(t_i,t_*)w_d^T(t_*,t_0)\right] \\ &= -\tilde{H}_i\int_{t_0}^{t_*}\int_{t_i}^{t_*}\Phi(t_*,\tau)Q(\tau)\delta(\tau-\tau')\Phi^T(t_*,\tau')\mathrm{d}\tau\mathrm{d}\tau' \\ &= -\tilde{H}_i\,Q_{*,i}\end{aligned} \tag{47}$$

where the minus sign arises from the change in direction of the inner integral over τ. Putting this together gives

$$P_{*|N} = \left(I_n - \sum_{i=1}^{N} K_i\tilde{H}_i\right)P_{*|0}\left(I_n - \sum_{i=1}^{N} K_i\tilde{H}_i\right)^T + \sum_{i=1}^{N} K_iR_iK_i^T$$

$$- \sum_{i,j=1}^{N} K_i\tilde{H}_iQ_{*,\min(i,j)}\tilde{H}_j^TK_j^T + \sum_{i=1}^{N}(K_i\tilde{H}_iQ_{*,i} + Q_{*,i}\tilde{H}_i^TK_i) \tag{48}$$

$$= P_{*|0} + \sum_{i,j=1}^{N} K_iW_{ij}K_j^T - \sum_{i=1}^{N}\left[K_i\tilde{H}_i(P_{*|0} - Q_{*,i}) + (P_{*|0} - Q_{*,i})\tilde{H}_i^TK_i^T\right], \tag{49}$$

where

$$W_{ij} \equiv \tilde{H}_i\left[P_{*|0} - Q_{*,\min(i,j)}\right]\tilde{H}_j^T + R_i\delta_{ij} = W_{ji}^T. \tag{50}$$

We now define the symmetric matrix $\tilde{W}$ as an $N \times N$ matrix of $m_i \times m_j$ blocks W_{ij}:

$$\tilde{W} = \begin{bmatrix} W_{11} & W_{12} & \dots & W_{1N} \\ W_{21} & W_{22} & \dots & W_{2N} \\ \vdots & \vdots & \ddots & \vdots \\ W_{N1} & W_{N2} & \dots & W_{NN} \end{bmatrix}, \tag{51}$$

The inverse $\tilde{W}^{-1}$ can also be written an $N \times N$ matrix of $m_i \times m_j$ blocks,

$$\tilde{W}^{-1} = \begin{bmatrix} [\tilde{W}^{-1}]_{11} & [\tilde{W}^{-1}]_{12} & \dots & [\tilde{W}^{-1}]_{1N} \\ [\tilde{W}^{-1}]_{21} & [\tilde{W}^{-1}]_{22} & \dots & [\tilde{W}^{-1}]_{2N} \\ \vdots & \vdots & \ddots & \vdots \\ [\tilde{W}^{-1}]_{N1} & [\tilde{W}^{-1}]_{N2} & \dots & [\tilde{W}^{-1}]_{NN} \end{bmatrix}, \tag{52}$$

and the relations $\tilde{W}\tilde{W}^{-1} = \tilde{W}^{-1}\tilde{W} = I$ imply that

$$\sum_{j=1}^{N} W_{ij}[\tilde{W}^{-1}]_{jk} = \sum_{j=1}^{N} [\tilde{W}^{-1}]_{ij} W_{jk} = \delta_{ik} I_{m_i}. \tag{53}$$

Now Eq. 49 can be written by completing the square as

$$\begin{aligned} P_{*|N} = P_{*|0} &- \sum_{i,j=1}^{N} (P_{*|0} - Q_{*,i}) \tilde{H}_i^T [\tilde{W}^{-1}]_{ij} \tilde{H}_j (P_{*|0} - Q_{*,j}) \\ &+ \sum_{i,j=1}^{N} \left\{ K_i - \sum_{k=1}^{N} (P_{*|0} - Q_{*,k}) \tilde{H}_k^T [\tilde{W}^{-1}]_{ki} \right\} W_{ij} \left\{ K_j - \sum_{k=1}^{N} (P_{*|0} - Q_{*,k}) \tilde{H}_k^T [\tilde{W}^{-1}]_{kj} \right\}^T \end{aligned} \tag{54}$$

If A and B are real symmetric matrices, we say that $A \geq B$ if the matrix $A - B$ is positive semidefinite. It is clear that

$$P_{*|N} \geq P_{*|0} - \sum_{i,j=1}^{N} (P_{*|0} - Q_{*,i}) \tilde{H}_i^T [\tilde{W}^{-1}]_{ij} \tilde{H}_j (P_{*|0} - Q_{*,j}) \tag{55}$$

in this sense, with equality if the measurement gains are chosen to be

$$K_i = \sum_{k=1}^{N} (P_{*|0} - Q_{*,k}) \tilde{H}_k^T [\tilde{W}^{-1}]_{ki}. \tag{56}$$

We will use these gains to achieve in this sense the minimum $P_{*|N}$, which can be expressed more compactly as

$$P_{*|N} = P_{*|0} - \sum_{j=1}^{N} K_j \tilde{H}_j (P_{*|0} - Q_{*,j}) \tag{57}$$

Sequential Form

Inversion of $\tilde{W}$ can be avoided by implementing a sequential estimation procedure. In developing a sequential estimator, it will be convenient to denote the gain matrices by $K_{i|k}$, where the index k is the number of measurements included in the update. The updates with $k-1$ and k measurements are thus

$$\hat{x}_{*|k-1} = \left(I_n - \sum_{i=1}^{k-1} K_{i|k-1} \tilde{H}_i \right) \hat{x}_{*|0} + \sum_{i=1}^{k-1} K_{i|k-1} y_i, \tag{58}$$

$$\hat{x}_{*|k} = \left(I_n - \sum_{i=1}^{k} K_{i|k} \tilde{H}_i \right) \hat{x}_{*|0} + \sum_{i=1}^{k} K_{i|k} y_i. \tag{59}$$

For a sequential method, we need to be able to write

$$\hat{x}_{*|k} = (I_n - K_{k|k} \tilde{H}_k) \hat{x}_{*|k-1} + K_{k|k} y_k. \tag{60}$$

Substituting Eq. 58 into Eq. 60 and comparing with Eq. 59 gives the consistency requirement*

$$K_{i|k} = (I_n - K_{k|k} \tilde{H}_k) K_{i|k-1}, \quad i < k. \tag{61}$$

To make further progress, we write

$$\tilde{W}_k = \begin{bmatrix} \tilde{W}_{k-1} & V_k \\ V_k^T & W_{kk} \end{bmatrix}, \tag{62}$$

where

$$V_k \equiv \begin{bmatrix} W_{1k} \\ W_{2k} \\ \vdots \\ W_{(k-1)k} \end{bmatrix} \tag{63}$$

Then the standard equation for the inverse of a partitioned matrix gives

$$\tilde{W}_k^{-1} = \begin{bmatrix} (\tilde{W}_{k-1} - V_k W_{kk}^{-1} V_k^T)^{-1} & U_k \\ U_k^T & (W_{kk} - V_k^T \tilde{W}_{k-1}^{-1} V_k)^{-1} \end{bmatrix}, \tag{64}$$

where

$$U_k = -\tilde{W}_{k-1}^{-1} V_k (W_{kk} - V_k^T \tilde{W}_{k-1}^{-1} V_k)^{-1} = -\tilde{W}_{k-1}^{-1} V_k [\tilde{W}_k^{-1}]_{kk}. \tag{65}$$

Comparison with Eqs. 50 and 55 with N replaced by $k-1$ shows that

$$W_{kk} - V_k^T \tilde{W}_{k-1}^{-1} V_k = \tilde{H}_k (\hat{P}_{*|k-1} - \hat{Q}_{*,k}) \tilde{H}_k^T + \hat{R}_k. \tag{66}$$

These relations give the gain matrix $K_{k|k}$, which is the only one needed for the sequential estimator, as

$$\begin{aligned} K_{k|k} &= \sum_{i=1}^{k} (P_{*|0} - Q_{*,i}) \tilde{H}_i^T [\tilde{W}_k^{-1}]_{ik} \\ &= \sum_{i=1}^{k-1} (P_{*|0} - Q_{*,i}) \tilde{H}_i^T [\tilde{W}_k^{-1}]_{ik} + (P_{*|0} - Q_{*,k}) \tilde{H}_k^T [\tilde{W}_k^{-1}]_{kk} \\ &= (P_{*|k-1} - Q_{*,k}) \tilde{H}_k^T [\tilde{W}_k^{-1}]_{kk} \\ &= (P_{*|k-1} - Q_{*,k}) \tilde{H}_k^T \left[\tilde{H}_k (P_{*|k-1} - Q_{*,k}) \tilde{H}_k^T + R_k \right]^{-1} \end{aligned} \tag{67}$$

*This condition can only be satisfied in the presence of process noise for $t_i \leq t_*$.

The third equality uses, for $i < k$,

$$[\tilde{W}_k^{-1}]_{ik} = [U_k]_i = -\sum_{j=1}^{k-1} [\tilde{W}_{k-1}^{-1}]_{ij} [V_k]_j [\tilde{W}_k^{-1}]_{kk} = -\sum_{j=1}^{k-1} [\tilde{W}_{k-1}^{-1}]_{ij} W_{jk} \tilde{W}_k^{-1}]_{kk}$$

$$= -\sum_{j=1}^{k-1} [\tilde{W}_{k-1}^{-1}]_{ij} \tilde{H}_j (P_{*,0} - Q_{*,j})\, \tilde{H}_k^T [\tilde{W}_k^{-1}]_{kk} \tag{68}$$

and then

$$\sum_{i,j=1}^{k-1} (P_{*|0} - Q_{*,i})\, \tilde{H}_i^T [\tilde{W}_{k-1}^{-1}]_{ij} \tilde{H}_j (P_{*|0} - Q_{*,j}) = P_{*|0} - P_{*|k-1}, \tag{69}$$

and the fourth equality uses Eq. 66. Equation 67 expresses $K_{k|k}$ in terms of only $P_{*|k-1}$ and quantities available at the measurement time t_k. To complete the development of the recursive estimator, we need a recursion relation for $P_{*|k}$. Using the consistency condition on the gains, Eq. 61, in Eq. 57 gives

$$\begin{aligned}
P_{*|k} &= P_{*|0} - \sum_{j=1}^{k} K_{j|k}\, \tilde{H}_j (P_{*|0} - Q_{*,j}) \\
&= P_{*|0} - K_{k|k}\, \tilde{H}_k (P_{*|0} - Q_{*,k}) - \sum_{j=1}^{k-1} K_{j|k}\, \tilde{H}_j (P_{*|0} - Q_{*,j}) \\
&= (I_n - K_{k|k}\, \tilde{H}_k) \left[P_{*|0} - \sum_{j=1}^{k-1} K_{j|k-1}\, \tilde{H}_j (P_{*|0} - Q_{*,j}) \right] + K_{k|k}\, \tilde{H}_k Q_{*,k} \\
&= (I_n - K_{k|k}\, \tilde{H}_k) P_{*|k-1} + K_{k|k}\, \tilde{H}_k Q_{*,k} \\
&= P_{*|k-1} - K_{k|k}\, \tilde{H}_k (P_{*|k-1} - Q_{*,k}).
\end{aligned} \tag{70}$$

Relation to the Kalman Filter

If we define

$$\tilde{P}_k = P_{*|k-1} - Q_{*,k}, \tag{71}$$

then Eq. 67 becomes

$$K_{k|k} = \tilde{P}_k\, \tilde{H}_k^T (\tilde{H}_k \tilde{P}_k\, \tilde{H}_k^T + R_k)^{-1} \tag{72}$$

and Eq. 70 becomes

$$\tilde{P}_{k+1} = (I_n - K_{k|k}\, \tilde{H}_k) \tilde{P}_k + Q_{*,k} - Q_{*,k+1} = (I_n - K_{k|k}\, \tilde{H}_k) \tilde{P}_k + Q_{k+1,k}, \tag{73}$$

which are the customary Kalman Filter equations, a result shown by Montenbruck.[11] It should be pointed out, though, that $\tilde{P}_k$ is not the covariance of any obvious error vector. However, if we further define

$$P_{k|k-1} = \Phi(t_k, t_*) \tilde{P}_k \Phi^T(t_k, t_*), \tag{74}$$

then equations (67) and (70) become, using the semigroup property of the state transition matrix,

$$K_{k|k} = \Phi(t_*, t_k) P_{k|k-1} H_k^T (H_k P_{k|k-1}\, H_k^T + R_k)^{-1} \equiv \Phi(t_*, t_k) \tilde{K}_k \tag{75}$$

and

$$P_{k+1|k} = \Phi(t_{k+1}, t_k)(I_n - \tilde{K}_k H_k)P_{k|k-1}\Phi^T(t_{k+1}, t_k) + \Phi(t_{k+1}, t_*)Q_{k+1,k}\Phi^T(t_{k+1}, t_*). \quad (76)$$

Notice that the tildes have been removed from the measurement sensitivity matrices. The latter equation can be written as the usual two-step Kalman filter process

$$P_{k|k} = (I_n - \tilde{K}_k H_k)P_{k|k-1} \quad (77)$$

$$P_{k+1|k} = \Phi(t_{k+1}, t_k)P_{k|k}\Phi^T(t_{k+1}, t_k) + \int_{t_k}^{t_{k+1}} \Phi(t_{k+1}, \tau)Q(\tau)\Phi^T(t_{k+1}, \tau)\mathrm{d}\tau, \quad (78)$$

where the expression for the process noise follows from Eq. 13. It is now easy to recognize $P_{k|k-1}$ and $P_{k|k}$ as the pre- and post-update covariances of the estimation error at the measurement time t_k.

We finally note that the update of the epoch state can be written as

$$\begin{aligned}\hat{x}_{*|k} &= \hat{x}_{*|k-1} + K_{k|k}(y_k - \tilde{H}_k \hat{x}_{*|k-1}) \\ &= \hat{x}_{*|k-1} + \Phi(t_*, t_k)\tilde{K}_k \left[y_k - H_k\Phi(t_k, t_*)\hat{x}_{*|k-1}\right], \end{aligned} \quad (79)$$

exactly as we would expect.

APPENDIX B: ERRATA FOR "GENERALIZED LINEAR COVARIANCE ANALYSIS"

This article was published in *The Journal of the Astronautical Sciences*, Vol. 57, Nos. 1 and 2, January–June 2009, pp. 233–260. It contains several errata:

Equation (69) should read

$$r = \tilde{H}e_*^- + u_d + v \quad (69)$$

The comment between equations (77) and (78) should read

"with $P_*^- = P(t_*^-)$,"

Equation (82) should read

$$= \begin{cases} Q_d(t_i, t_*)\Phi^T(t_j, t_i) & t_* < t_i \le t_j, \\ \Phi(t_i, t_j)Q_d(t_j, t_*) & t_* < t_j \le t_i, \\ \Phi(t_i, t_*)Q_d(t_*, t_j)\Phi^T(t_j, t_*) & t_i \le t_j < t_*, \\ \Phi(t_i, t_*)Q_d(t_*, t_i)\Phi^T(t_j, t_*) & t_j \le t_i < t_*, \\ 0 & \text{otherwise.} \end{cases} \quad (82)$$

Equations (86)–(88) should read

$$N_d(t) = \mathrm{E}\left[e_{w*}^+ w_d^T(t, t_*)\right] \quad (86)$$

$$= -\mathrm{E}\left[\tilde{S}_* \textstyle\sum_i K_i u_{di} w_d^T(t, t_*)\right] \quad (87)$$

$$= -\tilde{S}_* \textstyle\sum_i K_i H_i Q_d(t_*; t, t_i) \quad (88)$$

The line immediately above equation (94) should read

"at epoch. In equation (75) the matrix $(I_n - \tilde{S}_* \sum_i K_i \tilde{H}_i)$ is replaced by"

The assumption made below equation (74) that the errors in e_{a*}^+, e_{v*}^+, and e_{w*}^+ are uncorrelated is certainly valid if t_* is prior to all the measurements, so the results of the paper are equally valid in that case. If t_* is later than some or all of the measurements, however, it might be more reasonable to assume that e_{a*}^+ includes the process noise accumulated between the beginning of the observation span and t_*, in which case it has nontrivial correlations with e_{w*}^+. This modifies the manner in which process noise appears in the covariance analysis of the batch estimator, as shown in Appendix A. A fuller account will appear in a future paper.

REFERENCES

[1] J. R. Carpenter and F. L. Markley, "Sequential Probability Ratio Test for Collision Avoidance Maneuver Decisions," *Proceedings of the Kyle T. Alfriend Astrodynamics Symposium*, Univelt, 2010.

[2] R. Zanetti, M. Majii, R. H. Bishop, and D. Mortari, "Norm-Constrained Kalman Filtering," *Journal of Guidance, Control, and Dynamics*, Vol. 32, September–October 2009, pp. 1458–1465.

[3] A. Wald, *Sequential Analysis*. Dover Publications, 2004.

[4] R. G. Brown and P. Y. Hwang, *Introduction to Random Signals and Applied Kalman Filtering*. New York, NY: John Wiley and Sons, Inc., 3rd ed., 1997.

[5] D. G. Hull, *Optimal Control Theory for Applications*. Springer, 2003.

[6] D.-W. Gim and K. T. Alfriend, "State Transition Matrix of Relative Motion for the Perturbed Noncircular Reference Orbit," *Journal of Guidance, Control, and Dynamics*, Vol. 26, November-December 2003, pp. 956–971.

[7] J. L. Speyer and J. E. White, "Shiryayev Sequential Probability Ratio Test for Redundancy Management," *Journal of Guidance, Control and Dynamics*, Vol. 7, September–October 1984, pp. 588–.

[8] R. H. Battin, S. R. Croopnick, and J. E. Lenox, "The Epoch State Navigation Filter," *Journal of Guidance and Control*, Vol. 1, September–October 1978, pp. 359–364.

[9] R. G. Gottlieb, S. J. Sponaugle, and D. E. Gaylor, "Orbit Determination Accuracy Requirements for Collision Avoidance," *Space Flight Mechanics 2001*, Univelt, 2001.

[10] K. F. Gauss, *Theory of the Motion of the Heavenly Bodies Moving About the Sun in Conic Sections*. New York: Dover, 1963.

[11] O. Montenbruck, "An Epoch State Filter for use with Analytical Orbit Models of Low Earth Satellites," *Aerosp. Sci. Technol.*, Vol. 4, 2000, pp. 277–287.

[12] F. Hoots and R. L. Roehrich, "Models for Propagation of NORAD Element Sets," Tech. Rep. of Project Spacetrack No. 3, Aerospace Defense Command, United States Air Force, December 1980.

[13] F. L. Markley and J. R. Carpenter, "Generalized Linear Covariance Analysis," *Journal of the Astronautical Sciences*, Vol. 57, Jan–Jun 2009, pp. 233–260.